Overcoming Shockley−Queisser Limit Using Halide Perovskite Platform?

Kai Wang,[1,2*#] Luyao Zheng,[1#] Yuchen Hou,[1] Amin Nozariasbmarz,[1,2] Bed Poudel,[1,2*] Jungjin Yoon,[1] Tao Ye,[1] Dong Yang,[1] Alexej V Pogrebnyakov,[1,2] Venkatraman Gopalan,[1,2] Shashank Priya[1,2*]

[1]Department of Materials Science and Engineering, Pennsylvania State University, University Park, PA, 16802 USA

[2]Materials Research Institute, Pennsylvania State University, University Park, PA, 16802 USA

Abstract

Single-junction solar cells have a theoretical efficiency limit of 33.7%, with over 50% energy losses by thermalization and in-band transparency. Several strategies in engineering the photovoltaics (PVs) at device or system levels have been developed to reduce these losses and to break the Shockley–Queisser (SQ) limit efficiency while many solutions requires high manufacturing standard and deliver mild enhancement in efficiency. A breakthrough in addressing this problem can be found by materials engineering, which can overcome the conventional limitation of delicate PV materials and an inferior low efficiency baseline. Halide perovskite materials with simultaneously high efficiency and various material merits may provide the platform to overcome both thermalization and in-band transparency losses and thus possibly elevate the efficiency by two factors. For example, the long hot carrier lifetime in perovskite may make it possible to obtain a photovoltage of a cell exceeding active layer's bandgap or to execute a multi-exciton generation to double the photocurrent. A properly designed perovskite quantum system could overcome the in-band losses by mechanisms such as intermediate band pumping, multiple quantum well cascade, and photoferroic effect. Here we discuss the opportunity, feasibility and challenges of overcoming the SQ limit by using a perovskite material with designed properties.

#Equal contribution
*corresponding authors: KW (kaiwang@psu.edu); BP (bup346@psu.edu); SP (sup103@psu.edu)

1. Introduction

Utility-scale solar technique such as photovoltaics (PVs) have been recognized as a renewable energy technology with the potential to significantly contribute towards the future energy supply, and have been proven as the most pandemic resilient energy source in the year of 2020.[1] Based on a power-cost criterion,[2] PV techniques can be classified into three generations, where the 1st generation solar cells are based on single crystal gallium arsenide and silicon materials with a high cost of manufacturing, the 2nd generation are less-expensive polycrystalline and amorphous thin films, and the 3rd generation are lower cost but higher efficiency PV materials such as organics (OPV), natural dyes (DSSC), quantum dots (QD-PV) and halide perovskites (HP-PV). All three generations of solar cells have progressed rapidly in past few decades. The advancements in manufacturing technology are continuously reducing the levelized cost of electricity (LCOE) for 1st & 2nd generation PVs, moving the user cost towards retail electricity rate and gradually reaching the 'socket' parity.[3] For 3rd generation cells, novel low-cost PV materials processed using wet-chemistry are displaying efficiencies on the order of 18.2% for OPV and 25.5% for HP-PV,[4] respectively. A higher power conversion efficiency (PCE) could be a crucial lever for PV cost reduction, and a requirement in urban areas with limited space as it provides higher output power per unit area. Nevertheless, the ceiling for PV efficiency is given by Shockley–Queisser (SQ) theory, which applies to all these state-of-the-art (SOA) solar cells.[5]

The SQ limit refers to the maximum theoretical efficiency of a single-junction solar cell and is calculated by examining the amount of electrical energy extracted per incident photon. Using an AM 1.5 solar spectrum, a solar cell with an ideal bandgap light absorber (bandgap, E_g=1.4 eV) could have an upper limit on PCE of 33.7%,[6] *i.e.*, a maximum electrical power generation of 337 W m^{-2}. A major loss factor is related to the energy mismatch between broad wavelength distribution of sun light and the mono-bandgap of the light absorber in the cell. There are five dominant energy loss channels (**Figure 1A**), including (i) the coherent absorption-emission effect of solar cell (Kirchhoff's law of thermal radiation), (ii) Carnot loss by considering the heat engine operation between the heat source (*ca.* 6000 K) and the solar cell heat sink (*ca.* 300 K), (iii) Boltzmann loss by considering angular inequality of absorption and emission and thereby the entropy generation, (iv) thermalization loss from heat dissipation of hot carriers, and (v) in-band loss due to below E_g light-transparency of the absorber in cell. So far, several strategies have been developed to mitigate these losses. For example, light concentration can reduce the loss related to

Boltzmann entropy;[7] tandem/multi-junction cell can decrease the thermalization loss; equipping external accessories such as multiple photon up-conversion and down-conversion filters and construction of a thermophotovoltaic (TPV) system with thermal radiation regulators that could reconstruct the light spectrum being shed on the solar cell and thereby manage the thermalization and in-band losses.[4,8] Although these external spectral tuning methodologies could potentially enhance the PCE, the manufacturing cost of these complex photonic/thermal accessories represent a noticeable drawback. Seeking opportunities that are intrinsically part of the light harvesting material itself and revisiting scientific mechanisms to overcome the SQ limit through material-level engineering is of great interest among diverse communities. This emphasis will potentially drive the development of new PV techniques and trigger the evolution of the next generation of ultrahigh PCEs exceeding the SQ limit.

Recently, halide perovskites have emerged as phenomenal materials displaying many nontrivial properties including strong electron-phonon coupling induced slower cooling of hot carrier, inverse Auger process and thereby photocarrier multiplication,[9] intrinsic electric dipole polarization and thereby ferroelectric properties, along with other basic PV prerequisites such as large extinction coefficient in the visible range of the spectrum, long carrier diffusion length, and high charge carrier mobilities. In this perspective, building upon the perovskite platform we will discuss the opportunities, challenges and specific proposals for achieving PCEs exceeding the SQ limit.

2. Overcoming Thermalization Losses

In principle, there are five E_g-dependent intrinsic energy losses in a single junction solar cell. As can be seen in **Figure 1A**, thermalization ($T(Eg)$) and in-band loss (I(Eg)) represent the major loss pathways, accounting for over 50% of energy loss for the E_g ranging from 0.5 to 3.0 eV. The in-band loss corresponds to the transparency to photons with smaller energy than the bandgap, while the thermalization loss correlates with the nonequilibrium dynamics of photocarriers excited by photons of much higher energy than the bandgap followed by a quick cooling process downwards to the band edges (**Figure 1B**).[10] Before cooling, these high energy level charge carriers are usually termed as 'hot carriers', as they possess initial excess kinetic energies above the conduction or below the valence bands so that their initial temperatures are always above the 'lattice temperature'. The hot carriers usually have short lifetime in typical semiconductors (*e.g.*,

2 ps and 10 ps in GaAs and InN films, respectively).[11,12] While in halide perovskites, due to the strong electron-phonon coupling (Fröhlich interaction) and/or the carriers' polaronic nature, and the phonon bottleneck effect as well as many other potential mechanisms,[13] the hot carriers could have orders of magnitude longer lifetimes (*e.g.*, prior reports have revealed 1,000 ps in $FASnI_3$ films and > 2,500 ps in $MAPbI_3$ films, respectively).[14,15] In addition, recently the lower dimensional perovskites with both quantum and dielectric confinement even exhibit slower cooling of hot carriers (**Figure 1C**).[11,16,17] This can be ascribed to the quantization effects in these multiple quantum well (MQW)-structured quasi-2D perovskites, where nonequilibrium longitudinal optical (LO) phonons are confined within the quantum well region and reabsorbed by electrons, thus retaining the LO phonons in the quantum well region rather than consume it (*i.e.*, an enhanced hot electron-phonon bottleneck effect).[18]

In order to break the SQ limit and achieve an ultrahigh PCE, proper utilization of the hot carriers provides the opportunity to reduce the thermalization losses. There are two fundamental ways: one is to extract the hot carriers before they cool down to band edge and thereby producing open-circuit voltage (V_{OC}) hypothetically larger than E_g (*i.e.*, $V_{OC} > E_g$),[19] this will require an ultrafast (sub-ps) extraction process between perovskite and charge transfer layers; the other is to multiply the electron-hole pair through impact ionization and thus enhancing the photocurrent to exceed 100% external quantum efficiency (EQE) (*i.e.*, EQE > 1).[20] We will describe these two scenarios in the following subsections.

2.1 Ultrafast hot carrier extraction for photovoltage exceeding E_g ($V_{OC} > E_g$)

In order to achieve photovoltage exceeding E_g in a solar cell, the time of photocarriers transport within perovskite lattice matrix ($\tau_{e,TR}$ and $\tau_{h,TR}$) and their extraction at the perovskite/electron transfer layer (ETL) or hole transfer layer (HTL) ($\tau_{e,EX}$ and $\tau_{h,EX}$) must be faster compared to the cooling time of hot carriers (τ_{col}),[21] as well as a quick external collection at electrodes to minimize recombination losses. As can be seen in **Figure 2A**, the hot charge carriers could have a Boltzmann distribution of density of state (DOS), followed by cooling down towards the CBM and VBM with a time scale of 100 ps (this could be larger in halide perovskites). This time needs to be larger than the time for hot carrier transport within the perovskite and the time for extraction across the interfaces of perovskite/ETL and perovskite/HTL. Perovskites have shown long-range quasi-ballistic transport of hot carriers as large as 230 nm for $MAPbI_3$ within 300 fs[22], which is longer

than that of 20 nm for Si, 85 nm for GaAs, and 14 nm for GaN,[23] so that the transport time of hot carriers' drifting in perovskite layer with a typical thickness (*ca.* 500 nm) could be smaller than the τ_{col} ~100 ps.[21] Nevertheless, in real case the diffusion and scattering could significantly cool down the hot carriers. Si and GaAs have small nonequilibrium transport lifetime for hot carriers, with a value of a few ps. In contrast, hybrid perovskites can have long lived and non-diffusive transport due to 'polaron' formation by the electron-lattice deformation protection and thereby a long time of 10's of ps, coupled by a large polaron mobility over 100 $cm^2 V^{-1} s^{-1}$.[24] Assuming a cell with 500 nm thick perovskite being operated under maximal power point at bias of 0.9 V, the drift velocity of carrier can be estimated to 2×10^6 cm s^{-1}, and carrier generated in the center of the perovskite film travelling 250 nm (half of the thickness of 500 nm) to reach the electrode will need 1.4 ps (τ_{TR}). Thus, it is possible in perovskite to have τ_{TR} much smaller than τ_{col}.[21]

In terms of extraction across layer interface, ultrafast charge extraction at perovskite/ETL and perovskite/HTL interfaces have been demonstrated by techniques such as transient absorption spectroscopy and time-resolved terahertz spectroscopy. For example, it has been revealed that the electron ($\tau_{h,EX}$) and hole ($\tau_{h,EX}$) extraction at the perovskite/TiO_2 and perovskite/Spiro-OMeTAD interface could have a smaller time scale of less than 1 ps,[25] smaller than τ_{col}.[21] However, the relatively low Fermi level of TiO_2 and high Fermi level of Spiro-OMeTAD can only extract the cold carriers located at the band edges. In fact, ideal ETL/HTL materials for hot carrier solar cells may have a tunneling barrier with a resonant level that can only accept narrow bandwidth energies so as to protect the hot carriers from mixing with cold carriers and thereby minimizing the entropy production. Wide bandgap materials with narrow conduction and valence bands such as organic molecules, and quantum dots with discrete energy levels are optimal options.[26] So far, wide bandgap ETL materials such as Bphen (4,7-diphenyl-1,10-phenanthroline) (having a higher lowest unoccupied molecular orbital (LUMO) level than CBM of $MAPbBr_3$),[27] benzoquinone molecules,[28] and HTL such as phenothiazine (PTZ) and P3HT have been demonstrated to have an ultrafast charge transfer across the interface,[28,29] with a timescale from sub-picoseconds scale. Along with these ultrafast extraction capabilities, the ETL and HTL also need to have higher LUMO and deeper HOMO (highest occupied molecular orbitals) levels, than the CBM and VBM of the perovskite, respectively. Seeking such difunctional ETL/HTL materials might be guided by using the knowledge and materials inventory that have been well developed in the field of organic light emitting diode (OLED), where there are plenty of electron/hole injection buffer materials

with wide bandgap and decent energy band structures. **Figure 2A** also lists several typical ETL/HTL candidates with higher/deeper energy levels ranging from -3.2 to -5.7 eV. Overall, jointly considering the competition of hot carrier cooling time (τ_{col}) versus the total time for transport within the perovskite (τ_{TR}) and extraction across the interface (τ_{EX}) is the prerequisite for achieving the hot carrier solar cell (HCSC).[21] Realization of this $\tau_{col} > \tau_{TR} + \tau_{EX}$ meanwhile offer proper abovementioned energy band alignment by device structural engineering is one of area where future research could focus. One possible design could be a bulk heterojunction (BHJ) composite consisting of bi-continuous phases of perovskite and HTL (each phase having 10s nanometer scale, as schematized in **Figure 2B**), which is similar to the concept of BHJ organic photovoltaics (OPVs).[30] This could reduce the drifting length from 100's of nm to 10's of nm for the hot carrier within the perovskite and enhance the probability of hot hole extraction from perovskite to the HTL, while the remaining hot electrons could still transfer along the surface of perovskite phase to the cathode.[31] Nevertheless, one challenge in hot carrier solar cell with V_{OC} exceeding E_g is the photocurrent loss due to the coexistence of cold carriers. As shown in **Figure 2A**, before cooling, the hot carriers have a Boltzmann distribution spreading over several electron-volts, implying that the cold carriers are also inadvertently present in the perovskites. The broad solar spectrum also contains photons with energy slightly larger than the E_g, leading to the emergence of cold carriers located at the band edges. These cold carriers cannot be directly extracted to the ETL or HTL due to the energy level mismatch. For example, cold electrons need an extra energy ($\Delta E = CBM_{perovskite} - LUMO_{ETL}$) to reach the extractable level by ETL. Strong carrier-carrier/carrier-phonon scattering may provide the kinetic energy required to pump these cold carriers. An alternative way can be the utilization of multiple ETLs to have a 'funnel'-like CB band gradient (**Figure 2C**) to take advantages of both hot and cold carriers. These pathways will definitely require additional considerations such as higher illumination intensity/strong carrier-phonon interaction, complex quantum architectures, and sophisticated nanomanufacturing techniques. To summarize, in order to realize these hot carrier solar cells, the following requirements will need to be considered where future efforts could be paid, **(i)** a more slower cooling in perovskite light absorber, **(ii)** deep energy level of ETL and HTL to match with the Boltzmann distributions of density of state (DOS) of hot carriers in perovskite, **(iii)** ultrafast extraction at the perovskite/ETL and perovskite/HTL interface, and **(iv)** fast external transport and

collection at electrodes. Fulfilling these requirements, could enable realization of the equation $\tau_{col} > \tau_{TR} + \tau_{EX}$.[21]

Besides the above-mentioned minimization of $(\tau_{TR} + \tau_{EX})$, enlarging the cooling time, τ_{col},[21] is another option, as perovskites so far display an exciting baseline of τ_{col} towards 10^3 ps. Prior studies have reviewed the strategies for engineering a slower hot carrier cooling in perovskites.[23] The main strategies include:

(a) maintenance of longitudinal optical (LO) phonons so that the long-lived LO phonons could continuously reheat the carriers. **Figure 2D** proposes the LO phonon reheating loop for slowing the cooling. It starts from the energy transfer from hot electrons to LO phonons *via* Fröhlich interaction, followed by LO phonon relaxation to longitudinal acoustic (LA) phonons. The LA phonons could either propagate to far-field and dissipate heat to the ambient or upconvert to LO phonons by A-site organic cations with multiple low-energy co-vibrational optical modes (**Figure 2E**) that can overlap well with acoustic branches and facilitate the phonon up-conversion.[17] Blocking the relaxation from LO to LA phonons (**Figure 2D(ii)**) is one option to prolong the lifetime of LO phonons, which could be a good addendum to the phonon bottleneck effect. This will require a large phononic bandgap between LO and LA phonons. $MAPbI_3$ perovskites display a large energy gap between LO (8 meV) and LA (2.5 meV) photons, indicating it to be a good candidate. Further enlargement of the phononic bandgap can be achieved by compositional engineering to realize large atomic mass difference between the positively and negatively charged ions.[32] For example, by using heavier metal (Eu^{2+}, Tm^{2+}) B-site substitutional doping and lighter halogen (Cl, Br) X-site substitutional doping. Another option to retain the LO phonons is to block the LA phonon propagation (**Figure 2D(iii)**). Recently, our team has revealed ultralow thermal conductivity of 0.3 $Wm^{-1}K^{-1}$ from polycrystalline $MAPbI_3$ sample, lower than typical PV materials (*e.g.,* 130 $Wm^{-1}K^{-1}$ for silicon, 52 $Wm^{-1}K^{-1}$ for GaAs). This propagation blocking effect on LA phonons may in turn promote their up-conversion to the LO phonons[17] (**Figure 2D(iv)**) which then reheats the electrons (**Figure 2D(v)**). This low thermal conductivity is believed to be related with the dynamic motions (rotation and vibration) of the organic sublattice (*e.g.,* MA) and their interaction with the inorganic sublattice (*e.g.,* Pb-I octahedra) so that they can efficiently scatter the inorganic sub-lattice vibration modes.[33] To further lower the thermal conductivity, lattice engineering of perovskite can be a good approach. We have recently found that the vacancy

ordered double perovskite such as Cs_2PtI_6 and Cs_2SnI_6 can provide even lower thermal conductivity, reaching magnitude on the order of 0.2 $Wm^{-1}K^{-1}$.

(b) Atomic scale material engineering to render perovskites with smaller effective mass and stronger polaron screening effect. Theoretical calculation reveals that perovskite with smaller effective mass tends to have a slower cooling.[34] Perovskite could have smaller effective mass for carriers (0.07~0.16 for $CsSnI_3$), compared to silicon (~0.26) and GaAs (~0.34). The effective mass is related with the energy dispersion in the momentum space and thus determined by the band structure, especially the band edges. In perovskite, the band edges correspond to the Pb *s* and I *p* orbitals from the inorganic sublattice. This inorganic sublattice is usually regulated by the organic cations, although the latter merely contributes to the band edge. The fast-molecular reorientation of A-site organic cations could facilitate the polaron formation with the electrons[35] and impart a screening effect to protect the hot carriers. Together, these potential pathways could be good criterions for down-selecting design and the optimal composition discovery *via* neuromorphic computing-based material exploration techniques[36].

(c) Structural and morphological engineering to maintain the nonequilibrium phonon populations. MQW structures in quasi-2D perovskites[37] are good examples to confine the phonons and reduce the hot carrier diffusion *via* the organic layer blocking effect as well as thus induced quantum- and dielectric- confinement.[38] Synergistic effects of formation of polarons,[39] Auger heating,[40] and hot-phonon bottleneck[11] can boost the cooling time towards orders of magnitude higher than that in typical semiconductors. And recently, new insights such as spin-degenerate band splits or the Rashba band splitting effect can further tune the cooling rate in those MQW quasi-2D perovskites.[41] Nevertheless, in these 2D perovskite where the QW becomes narrower, the easier formation of exciton state with higher exciton-binding energy will tend to have a stronger radiant recombination pathway, which is beneficial for light-emitting but harmful here for solar cell application. In parallel to these MQW, nanocrystals such as quantum dots (QD) could be an alternative way to maintain the slow cooling but with a tunable mild exciton binding energy depending on the QD size. While the inevitable chemical ligands and defects at the QD surface need to be well passivated to minimize the Shockley–Read–Hall (SRH) recombination (i.e., the trap-assisted recombination). Overall, invoking the quantum confinement without introducing extra issues of radiant (due to strong exciton binding energy) or non-radiant (SRH) recombination,

remains challenging in these 'fragile' perovskite materials, which may rely on innovations in nano-fabrication toolbox or breakthroughs in defect-free perovskite assembly techniques.

(d) At device level, not only the abovementioned retainment of hot carriers in perovskite but also a quick extraction and well retainment of hot carriers in HTL and ETL is important. So far, the most commonly used HTL and ETL materials do not have deep energy level so that most as extracted carriers are the 'cold carriers' that fail to generate a V_{OC} exceeding the E_g. Proper material selection and device reconstruction (e.g., **Figs. 2A-C**) may provide potential strategies to real device.

2.2 Ultrahigh photocurrent with EQE exceeding 100% (EQE > 1)

Splitting one hot electron-hole pair into two or more pairs could be realized through impact ionization (**Figure 3A**).[20] To obtain such an 'inverse Auger' effect, the impact ionization rate needs to be faster than the cooling rate so that multiple exciton generation (MEG) could lead to an EQE over 100% under certain wavelength.[42] Traditional PV semiconductors in bulk form exhibit negligible MEG due to a weak carrier-carrier interaction, and usually with a high photon energy threshold (> $4E_g$) to trigger the MEG. Quantizing the energy level and spatially confining the hot carriers could lift the momentum conservation and enhance the many-body effects among carriers, and consequently higher MEG yields are observed in their QD systems.[43] Several research groups so far have observed the MEG in perovskite nanocrystals.[9,44] Particularly, low threshold energy of $2.25E_g$ and great slope efficiency (η) of 75% has been reported in $FAPbI_3$ nanocrystals, higher than those in PbS or PbSe.[9] The η is defined by Beard and Nozik *et al.*,[45] as the minimum energy required to produce an exciton (*i.e.*, the band gap) over the actual amount of energy required to produce an additional exciton *via* MEG. In an ideal case, η reaches the maximal value of 1, suggesting minimized thermal losses to zero whereby one photon with an energy value of $2E_g$ can lead to two excitons with energy of E_g. The η can be obtained from the plot of QY (quantum yield) vs. $h\nu/E_g$. **Figure 3A(ii)** compares the η between perovskites and typical quantum materials, where the $CsPbI_3$ nanocrystals exhibit a decent η to 98%, indicating a highly efficient MEG. Although these studies provide exciting material-oriented foundations for MEG solar cell, there is a lack of device-level demonstrations. In the device environment, a slower hot carrier cooling (*i.e.,* a larger τ_{col}, can be found as discussed in **Section 2.1**) is of great importance to construct a sufficient large time frame for the MEG.[21] In typical IV–VI QD MEG solar cells, methodologies such as tailoring

the QD ligand chemistry, constructing a core-shell architecture, and selecting proper QD materials have been demonstrated to enhance the MEG effect. However, the inferior charge transport and extraction remains the major barrier for achieving high PCE in QD solar cells, due to the under-coordinated surface atoms and thus induced in-band surface states that will trap a large portion of photocarriers and consequently diminish the V_{OC}. Similar problems also exist in perovskite QD solar cells leading to a fair PCE of <15% (vs. 25% from polycrystalline perovskites).[46] Surface passivation using lattice-matching material or ligand modification could be effective way to reduce the loss and would need further efforts to optimize the inter-QDs charge transport.

An alternative quantum form is a quasi-2D MQW perovskite. PCE of 18.48% has been demonstrated in $(GA)(MA)_nPb_nI_{3n+1}$ (n = 3) MQW solar cells.[47] Similar to QD, perovskite MQW structure also manifests the quantum confinement effect, electron-phonon coupling, and other conditions for hot carrier cooling. In quasi-2D perovskite, there is a flexibility to tune the thickness of QW (*via* enlarging the index *n*) and QB (quantum barrier, *via* using A-site organic spacer of different sizes) individually. So far, many quasi-2D perovskites ranging from MQW (with thick barrier so that neighboring QWs are electronically isolated) to superlattice (with thin barrier so that charge carriers can have efficient out-of-plane transport *via* the minibands) have been reported. However, there are a limited number of studies on the MEG effect in quasi-2D MQW/superlattice perovskites. Compared to inter QD losses in the QD MEG solar cell, the quasi-2D perovskites can be vertically aligned within the device (**Figure 3B(i)**) so that the photocarriers could transfer within the 2D QW plane, thereby reducing losses. Discrete quantized energy levels are also present in quasi-2D perovskites, which has been observed both theoretically and experimentally. A cooling time of 720 fs in $(EA)_2PbI_4$ 2D perovskite has been reported.[48] This number is much smaller than nanocrystals of $MAPbI_3$, which could be related to restriction of the dynamics of the large A-site cation. In order to realize the MQW MEG solar cell, an optimal candidate could be the quasi-2D perovskites with FA or MA cations of higher dynamic freedoms located in the QW region, and a thick barrier consisting of large organic cations with a highly axial rotational nature. The thicker QW region enables a smaller exciton binding energy and thereby an easier separation into free carriers at room temperature, while the thicker barrier enables a sufficient decoupling of wavefunction of charge carriers from neighboring QW. From device level, this quasi-2D perovskites need to be inserted between asymmetric electrodes with an edge-on stacking to ensure efficient charge transport perpendicular to the electrode plane (**Figure 3B(ii)**).

In parallel to the abovementioned impact ionization in pure perovskite quantum system, another way to realize the MEG could be the singlet fission (SF) in a mixed system consisting of perovskite and organic chromophores. The SF typically occurs in certain organic chromophores (*e.g.,* pentacene, rubrene, perylene, *etc.*) where one excited singlet-state (S_n) transforms into two triplet states (T_1) upon close interaction with a ground-state (S_0) molecule of the same kind (**Figure 3C**). This SF process could occur at a timescale of sub-100 fs with a quantum yield of 200%. By incorporating SF chromophores into solar cells, total exciton yields of 133%, EQE of 130%, and IQE (internal quantum efficiency) of 170% has been observed in tetracene sensitized silicon solar cells,[49] pentacene incorporated organic solar cell,[50] and TIPS–pentacene/PbSe QD solar cells,[51] respectively. These breakthrough conceptualizations are one of the early successful attempts in realizing the MEG at device level. Projecting to future, it would take developmental time to realize a device to practically approach to and even exceed its SQ limit, where research areas such as improvement of MEG quantum yield, bandgap design to maximize light usage and minimize the optical loss, and material nano-structural and device structural engineering to reduce SRH losses can be focused on to accelerate this implementation.

In perovskite, most of these type researches are at the material level. For example, excited state transfer between perovskite and SF chromophores has been optically probed,[52,53] while using SF to boost photocurrent of perovskite solar cell devices remains unexplored. To construct such device, in principle, there could be either electrically or energetically utilization of SF effect. As shown in **Figure 3D**, long wavelength light of smaller photon energy can be absorbed in deeper perovskite layer while the short wavelength light is absorbed by the SF chromophore whereby forming two T_1 excitons from one S_n exciton. The first electrical approach accounts for charge transfer across the SF chromophore/perovskite interface that the as-formed T_1 excitons diffuse to this interface and dissociate into free electrons and holes, followed by individual transfer to electrodes (**Figure 3D(i)**). This will require a good heterojunction between the chromophore and perovskite, where there should be minimized energy losses from band offsets and minimized defect density as well as recombination loss. Meanwhile, as the chromophore also acts as the HTL (**Figure 3D(i)**), it also requires good hole mobility for these chromophore materials. So far, there have been few relevant studies exploring the chromophore/perovskite heterojunction and little is known about this type of mechanism. In parallel, the second energetic approach is to transfer the T_1 excitons across the interface *via* an energy transfer mechanism (**Figure 3D(ii)**). Recently, an

efficient Dexter energy transfer has been observed at the pentacene/$CsPbBr_3$ QD interface.[52] In that work, singlet exciton transferred from perovskite to pentacene, followed by SF in pentacene. This is an important perspective for utilizing SF, but may not likely to surpass the SQ limit because in real device the photovoltage of the T_1 excitons is half of that of S_1 and there are no additional excitons generated by any short wavelength light. Instead, a proper design needs exciton transfer from chromophore to perovskite, where lights of different photon energies are separately absorbed by chromophore and perovskite. For example, in **Figure 3D(ii)**, chromophore first absorbs short wavelength light and induces the SF to produce T_1 excitons, which transfer to perovskite *via* energy transfer process at the interface. After that, the exciton in perovskite can dissociate into free carriers due to low exciton binding energy in perovskite environment and can be further collected by electrode separately. This is a typical approach for SF sensitized Si solar cell and usually in a parallel device structure.[49] In conventional SF chromophore sensitized QD systems such as pentacene/PbSe and tetracene/PbS, the triplet energy transfer efficiency could reach to 100% across the interface *via* a Dexter process.[54] Normally, energy transfer is limited to distances of less than 10 nanometers and to sufficiently ensure the transfer efficiency a heterojunction with the aim of increased interfacial area needs to be considered. Additionally, whether this triplet transfer across the chromophore/perovskite interface also exhibits such a high efficiency and how such interface is present in device to utilize this SF for doubling the EQE still remains to be explored in perovskite solar cells.

3. Overcoming In-Band Losses

The in-band losses arise from the transparency of photons with energy smaller than the bandgap. Utilization of in-band light could be realized *via* two-photon absorption (or multi-photon absorption) or sequential sub-band absorption with the assistance of an intermediate miniband (IB). The former usually needs much higher light intensity than the solar illumination. The latter has been proposed as the intermediate band solar cells which could be regarded as an analogy to a set of two sub-cells connected in series (corresponding to the VB–IB and IB–CB transitions) and one in parallel (corresponding to the VB–CB transition) (**Figure 4A**). An optimal IB solar cell requires a total E_g of 1.95 eV to split sub-bandgaps of 0.71 eV and 1.24 eV, which will result in about 63% PCE under concentrated sun light (46,050 suns).[55] Although concerns of non-radiative recombination caused by the IB centers, and material embodiment remains to be carefully refined,

many efforts have been made on the 1st-generation photovoltaic materials. Particularly in order to construct an IB, incorporating QDs (with discretized levels) or impurities (*e.g.,* metal elements with partially filled *d* orbitals) and doping could intentionally invoke IB in III–V, II–VI, silicon, chalcopyrite semiconductors. Nevertheless, those IB solar cells are still at early stages by exhibiting not sufficient efficiencies.[56]

Perovskites have been predicted with an IB fingerprint in derived structures such as Cs_2SnI_6 double perovskite, 0-dimensional (0D) $EtPySbBr_6$ perovskites,[57,58] Co-doped $MAPbI_3$ and Mn-doped $CsPbI_2Br$.[59,60] While so far, most calculations indicate that these IB are flat and not likely to have electrons (empty band), which could induce severe recombination loss rather than sequential IB pumping. Following this scenario, it is necessary to have the IB with partially filled orbitals with presence of both empty states to receive electrons pumped from VB and full states to supply them to further pump to CB. Searching for perovskite material with this ideal IB structure needs to consider the electron configuration of the dopant metal element. An ideal candidate needs to render a half-filled IB to maximize the photoexcitation efficiency. One good example could be the Cr, Mo, In, or Ga doped $CsPbX_3$ (X = Cl, Br, I), which displays half-filled IB upon partial density of states (PDOS) analysis.[61] Particularly, Ga or In doped $CsPbCl_3$ with robust half-filled IB are good candidates based on calculation (**Figure 4B**). Properly tuning the doping concentration to ~8% could render an optimal theoretical IB bandwidth and thereby increase limit for PCE to ~55% for solar cells. Nevertheless, no experimental data has been collected for this scenario.

Using confined states of quantum material or incorporation of QDs in a wider E_g matrix to form periodic cascade energy levels is another way to induce IB (**Figure 4C**).[62,63] Quasi-2D MQW perovskite could be a good candidate in principle. While most existing quasi-2D perovskites have the organic barrier layers of much larger bandgap of exceeding 4 eV (that is, only responsible for absorption below 300 nm) and exhibit insulative nature. Replacing these A-site insulating cations with π-conjugated organics could be a possible solution. This will need a delicate design of the barrier bandgap, QW bandgap, as well as their cascaded band diagram and thickness of each quantum region. Alternatively, another way to construct the IB is to make a 'Plum pudding'-like composite with QDs embedded in a perovskite matrix, where QDs provide the IB for the wide E_g perovskite, which takes advantage of the tunability of perovskite's bandgap. This concept is inspired by the seminal work of IB solar cell in the year of 2007, where molecular beam epitaxy has been used to grow InAs QDs in a matrix of GaAs in the Stranski–Krastanov mode. However,

in the traditional material systems, lattice mismatch between QDs and matrix could trigger several issues and defects that significantly limit the PCE. One solution is to use colloidal QDs which however are difficult to be processed in the traditional semiconducting matrixes. In comparison, solution processed perovskites provide the opportunity to grow the Plum pudding composite with embedded QDs. Recently, IB solar cell using PbS QDs embedded in $MAPbBr_3$ *via* a wet chemistry method has been reported to display the IB-assisted two-step photon absorption,[63] and thus a good proof of concept demonstration of IB solar cell. While losses from charge transport, defects and interfaces induced recombination, are significantly larger than the IB gains, this consequently leads to a low PCE level of <1%.

In principle, abovementioned IB solar cells can be extended to multiple intermediate minibands. However, introducing more quantized intermediate states will also constrain the light absorption efficiency, and needs a joint consideration on the mutual interactions between different states. This sets up several restrictions on PCE improvements in theory. Experimentally, IB solar cell using III–V and other traditional material systems have not displayed exciting results. Wet chemistry and chemical flexibility (easiness in doping, compositional engineering and synthesis) of perovskite endow a good opportunity for developing IB solar cells, but significant challenges remain simultaneously.

4. Photoferroics

Halide perovskites with large dipole polarization from A-site molecules, could be a ferroelectric material. The spontaneously polarized ferroelectric domains could induce internal electric fields at the domain walls that can separate photogenerated excitons into free charges, and segregate the transport of the free charges to reduce recombination rates. This has been regarded as the working mechanism for oxide perovskite ferroelectrics such as $BiFeO_3$ (BFO), where high V_{OC} thousand times larger than E_g has been observed but at expense of a very small photocurrent. These conventional ferroelectric ceramics typically exhibit relatively large bandgap (e.g., 2.2 eV of BFO), making them insulative and so as a low J_{SC}. In contrast, halide perovskite can be designed to hypothetically have a proper semiconducting feature with optimal bandgap and simultaneously an intrinsic molecular polarization. Such ferroelectric and photovoltaic duality could provide the way towards ultrahigh efficiency photoferroics. In principle, the presence of domain wall under certain molecular alignment could reduce the E_g by 20−40% at the wall of halide perovskite.[64] Properly

taking advantage of this localized E_g shrinkage may possibly enhance the absorption, as schematically described in **Figure 4D**. Nonetheless, in the most commonly used efficient perovskites such as FA or MA-based lead iodide, whether the ferroelectricity is present or not, is under debate. It is expected that by introducing large dipole A-site cations, strong ferroelectric behavior could emerge. However, most of the existing ferroelectric halide perovskite materials have wide E_g with a more insulating attribute and are not likely to deliver high PCEs. At device level, other strategies utilizing electrically asymmetric functional materials such as polar metal[65] may help to introduce PV effect at other interface or domain walls but remain further investigations.

5. Summary and outlook

Other extrinsic scenarios such as incorporation of up- and down- conversion materials, solar-thermal conversion (photovoltaics, thermionic), and multijunction architectures are mostly included at the system-level and thus not discussed here. It should also be noted that halide perovskite also displays high Seebeck coefficient, but the relatively low electrical conductivity limits their applications in thermoelectric (TE) solar-heat conversion. Interestingly, perovskite could have charge carrier concentration increase by four-order-of-magnitude under illumination and thus higher ZT value could be expected under such circumstances. The TE/PV tandem solar harvester has been proposed yet still on the way to an ultrahigh PCE.

We have discussed the potential pathways for overcoming the SQ limit by focusing on the engineering of halide perovskite materials. The characteristically slow cooling of hot carrier in perovskite provides a great opportunity to fabricate realistic hot carrier solar cells with V_{OC} exceeding E_g, and MEG solar cells with EQE exceeding 100%. Additionally, MQW and QD perovskites with quantized electronic band structure could further enhance the hot carrier lifetime, MEG efficiency and possibly be the platform for the next-generation solar cell with an iconic PCE over the limit of 33.7%. This will not only require good properties at material level, but also a delicate arrangement at device level in terms of interfacial extraction (*e.g.,* resonant transport through nanostructures for hot carrier), transport (*e.g.,* decreased defect or phonon scattering), and collection efficiencies (semiconductor-metal contact), as well as absorptions (antireflection and plasmonic enhancement). The materials and device architectures to *exceed* the SQ limit can be distinctly different from those of traditionally used to *approach* the limit. In fact, in the past decade, much endeavours adopt the classic p-i-n or n-i-p architectures using commonly used ETL and HTL

such as SnO_2 and Spiro-OMeTAD respectively to continuously approaching the limit (in the last year, this has been progressed to a highest PCE of 25.8%[66]). Nevertheless, overcoming the barrier of SQ limit may need innovations in both materials and device architectures. In most conventional case, both carrier generation and extraction are considered in an equilibrium condition and most efforts are paid on the minimization of losses within this statistic condition, such as energy level alignment, carrier transport facilitation, and interface optimization. Shifting towards device to exceed the SQ limit, nonequilibrium process at smaller timeframe (i.e., femtosecond to picosecond level) and a dynamic model with temporal variants need to be considered since many abovementioned mechanisms take advantages of the hot carrier whose lifetime sits within this temporal range. Thus, there will need much attentions on the ultrafast process across the interface as well as innovative designs and trial & error efforts to implement these mechanisms into real device. In brief, shifting towards new device/material designs to maximize the functionality of the perovskite material for the overcoming of SQ limit remains challenging, but of high payback simultaneously. Instead of converging efforts to optimize the PCE to approach the limit, diversifiedly exploring the opportunities out of the box need to be encouraged. As the perovskite materials already displayed as good platform, and the prior endeavours in the past decade have provided the knowledgebase and learnings, upon these foundations it might be a good timing to consider using perovskite as the material platform to exceed the SQ limit.

From manufacturing perspective, material development and engineering could possibly overcome the technical barrier. For example, so far four-junction solar cells set up the upper limit of 46% for photovoltaic technology.[67] In principle, increasing the number of junctions to infinity could most efficiently manage the heat and transparency losses and thereby a higher PCE of 86.2% can be achieved,[68] however, this is extremely challenging in terms of manufacturing. While solutions might be hidden at material level. Materials with controllable effective mass and band diagrams could potentially allow a hot carrier solar cell (equivalent to that of a tandem stack with infinite number of sub-cells) to have a limiting PCE of 86.8%.[69] The state-of-the-art perovskite has been engineered to have minimal losses at mesoscale across grain boundary, interface and heterojunctions, providing a high PCE baseline of 25.5%. It exhibits many material merits not only in terms of physical properties but also in chemical tunability and easy manufacturing. Further material and device innovations built on this platform are anticipated to overcome the SQ limit.

Acknowledgement:

K.W. and Y.H. acknowledge the support from Air Force Office of Scientific Research (award number FA9550-17-1-0341). S.P. acknowledges the support through the Office of Naval Research through award number N00014161304. V.G acknowledges support from the Department of Energy grant DE-SC0012375.

References

1. Global Industry Analysts, I. (2021). Solar Cells and Modules - Global Market Trajectory & Analytics.
2. Green, M.A. (2001). Third generation photovoltaics: Ultra-high conversion efficiency at low cost. Prog. Photovoltaics Res. Appl. *9*, 123–135.
3. Hagerman, S., Jaramillo, P., and Morgan, G. (2014). What is "Socket" Parity and is Rooftop Solar PV There Yet Without Subsidies?
4. Green, M., Dunlop, E., Hohl-Ebinger, J., Yoshita, M., Kopidakis, N., and Hao, X. (2021). Solar cell efficiency tables (version 57). Prog. Photovoltaics Res. Appl. *29*, 3–15.
5. Shockley, W., and Queisser, H.J. (1961). Detailed balance limit of efficiency of p-n junction solar cells. J. Appl. Phys. *32*, 510–519.
6. Rühle, S. (2016). Tabulated values of the Shockley–Queisser limit for single junction solar cells. Sol. Energy *130*, 139–147.
7. Hirst, L.C., and Ekins-Daukes, N.J. (2011). Fundamental losses in solar cells. Prog. Photovoltaics Res. Appl. *19*, 286–293.
8. Zhou, Z., Chen, Q., and Bermel, P. (2015). Prospects for high-performance thermophotovoltaic conversion efficiencies exceeding the Shockley-Queisser limit. Energy Convers. Manag. *97*, 63–69.
9. Li, M., Begum, R., Fu, J., Xu, Q., Koh, T.M., Veldhuis, S.A., Grätzel, M., Mathews, N., Mhaisalkar, S., and Sum, T.C. (2018). Low threshold and efficient multiple exciton generation in halide perovskite nanocrystals. Nat. Commun. *9*, 637553.
10. Mićić, O.I., Cheong, H.M., Fu, H., Zunger, A., Sprague, J.R., Mascarenhas, A., and Nozik, A.J. (1997). Size-dependent spectroscopy of InP quantum dots. J. Phys. Chem. B *101*, 4904–4912.
11. Yang, Y., Ostrowski, D.P., France, R.M., Zhu, K., van de Lagemaat, J., Luther, J.M., and Beard, M.C. Observation of a hot-phonon bottleneck in lead-iodide perovskites. *10*, 53–59.
12. Chen, F., Cartwright, A.N., Lu, H., and Schaff, W.J. (2003). Time-resolved spectroscopy of recombination and relaxation dynamics in InN. Appl. Phys. Lett. *83*, 4984–4986.
13. Van Vleck, J.H. (1941). Paramagnetic relaxation and the equilibrium of lattice oscillators.

Phys. Rev. *59*, 724–729.

14. Bretschneider, S.A., Laquai, F., and Bonn, M. (2017). Trap-Free Hot Carrier Relaxation in Lead-Halide Perovskite Films. J. Phys. Chem. C *121*, 11201–11206.

15. Fang, H.H., Adjokatse, S., Shao, S., Even, J., and Loi, M.A. (2018). Long-lived hot-carrier light emission and large blue shift in formamidinium tin triiodide perovskites. Nat. Commun. *9*, 1–8.

16. Jia, X., Jiang, J., Zhang, Y., Qiu, J., Wang, S., Chen, Z., Yuan, N., and Ding, J. (2018). Observation of enhanced hot phonon bottleneck effect in 2D perovskites. Appl. Phys. Lett. *112*, 143903.

17. Yang, J., Wen, X., Xia, H., Sheng, R., Ma, Q., Kim, J., Tapping, P., Harada, T., Kee, T.W., Huang, F., *et al.* (2017). Acoustic-optical phonon up-conversion and hot-phonon bottleneck in lead-halide perovskites. Nat. Commun. *8*, 1–9.

18. Campos, V.B., Das Sarma, S., and Stroscio, M.A. (1992). Phonon-confinement effect on electron energy loss in one-dimensional quantum wires. Phys. Rev. B *46*, 3849–3853.

19. Ross, R.T., and Nozik, A.J. (1982). Efficiency of hot-carrier solar energy converters. J. Appl. Phys. *53*, 3813–3818.

20. Landsberg, P.T., Nussbaumer, H., and Willeke, G. (1993). Band-band impact ionization and solar cell efficiency. J. Appl. Phys. *74*, 1451–1452.

21. Boudreaux, D.S., Williams, F., and Nozik, A.J. (1980). Hot carrier injection at semiconductor-electrolyte junctions. J. Appl. Phys. *51*, 2158–2163.

22. Guo, Z., Wan, Y., Yang, M., Snaider, J., Zhu, K., and Huang, L. (2017). Long-range hot-carrier transport in hybrid perovskites visualized by ultrafast microscopy. Science *356*, 59–62.

23. Li, M., Fu, J., Xu, Q., and Sum, T.C. (2019). Slow Hot-Carrier Cooling in Halide Perovskites: Prospects for Hot-Carrier Solar Cells. Adv. Mater. *31*, 1802486.

24. Frost, J.M. (2017). Calculating polaron mobility in halide perovskites. Phys. Rev. B *96*, 195202.

25. Wang, K., Yang, D., Wu, C., Sanghadasa, M., and Priya, S. (2019). Recent progress in fundamental understanding of halide perovskite semiconductors. Prog. Mater. Sci. *106*, 100580.

26. Li, J.S., Chen, J.X., Lin, L.W., Li, Z.T., Tang, Y., Yu, B.H., and Ding, X.R. (2015). A Detailed Study on Phosphor-Converted Light-Emitting Diodes with Multi-Phosphor Configuration Using the Finite-Difference Time-Domain and Ray-Tracing Methods. IEEE J. Quantum Electron. *51*.

27. Li, M., Bhaumik, S., Goh, T.W., Kumar, M.S., Yantara, N., Grätzel, M., Mhaisalkar, S., Mathews, N., and Sum, T.C. (2017). Slow cooling and highly efficient extraction of hot carriers in colloidal perovskite nanocrystals. Nat. Commun. *8*, 1–10.

28. Sarkar, S., Ravi, V.K., Banerjee, S., Yettapu, G.R., Markad, G.B., Nag, A., and Mandal,

P. (2017). Terahertz Spectroscopic Probe of Hot Electron and Hole Transfer from Colloidal CsPbBr3 Perovskite Nanocrystals. Nano Lett. *17*, 5402–5407.

29. Shen, Q., Ripolles, T.S., Even, J., Zhang, Y., Ding, C., Liu, F., Izuishi, T., Nakazawa, N., Toyoda, T., Ogomi, Y., *et al.* (2018). Ultrafast selective extraction of hot holes from cesium lead iodide perovskite films. J. Energy Chem. *27*, 1170–1174.

30. Huang, Y., Kramer, E.J., Heeger, A.J., and Bazan, G.C. (2014). Bulk heterojunction solar cells: Morphology and performance relationships. Chem. Rev. *114*, 7006–7043.

31. Lee, M.M., Teuscher, J., Miyasaka, T., Murakami, T.N., and Snaith, H.J. (2012). Efficient hybrid solar cells based on meso-superstructured organometal halide perovskites. Science *338*, 643–647.

32. Conibeer, G.J., König, D., Green, M.A., and Guillemoles, J.F. (2008). Slowing of carrier cooling in hot carrier solar cells. Thin Solid Films *516*, 6948–6953.

33. Hata, T., Giorgi, G., and Yamashita, K. (2016). The Effects of the Organic-Inorganic Interactions on the Thermal Transport Properties of $CH_3NH_3PbI_3$. Nano Lett. *16*, 2749–2753.

34. Fu, J., Xu, Q., Han, G., Wu, B., Huan, C.H.A., Leek, M.L., and Sum, T.C. (2017). Hot carrier cooling mechanisms in halide perovskites. Nat. Commun. *8*, 1–9.

35. Zheng, F., and Wang, L. (2019). Large polaron formation and its effect on electron transport in hybrid perovskites. Energy Environ. Sci. *12*, 1219–1230.

36. Hou, Y., Wu, C., Yang, D., Ye, T., Honavar, V.G., Duin, A.C.T. van, Wang, K., and Priya, S. (2020). Two-dimensional hybrid organic–inorganic perovskites as emergent ferroelectric materials. J. Appl. Phys. *128*, 060906.

37. Chen, Y., Sun, Y., Peng, J., Tang, J., Zheng, K., and Liang, Z. (2018). 2D Ruddlesden–Popper Perovskites for Optoelectronics. Adv. Mater. *30*, 1703487.

38. Yin, J., Maity, P., Naphade, R., Cheng, B., He, J.-H., Bakr, O.M., Brédas, J.-L., and Mohammed, O.F. (2019). Tuning Hot Carrier Cooling Dynamics by Dielectric Confinement in Two-Dimensional Hybrid Perovskite Crystals. ACS Nano *13*, 12621–12629.

39. Miyata, K., Meggiolaro, D., Trinh, M.T., Joshi, P.P., Mosconi, E., Jones, S.C., Angelis, F. De, and Zhu, X.-Y. (2017). Large polarons in lead halide perovskites. Sci. Adv. *3*. e170121.

40. Fu, J., Xu, Q., Han, G., Wu, B., Huan, C.H.A., Leek, M.L., and Sum, T.C. (2017). Hot carrier cooling mechanisms in halide perovskites. Nat. Commun. 2017 81 *8*, 1–9.

41. Yin, J., Naphade, R., Maity, P., Gutiérrez-Arzaluz, L., Almalawi, D., Roqan, I.S., Brédas, J.-L., Bakr, O.M., and Mohammed, O.F. (2021). Manipulation of hot carrier cooling dynamics in two-dimensional Dion–Jacobson hybrid perovskites via Rashba band splitting. Nat. Commun. 2021 121 *12*, 1–9.

42. Semonin, O.E., Luther, J.M., Choi, S., Chen, H.Y., Gao, J., Nozik, A.J., and Beard, M.C.

(2011). Peak external photocurrent quantum efficiency exceeding 100% via MEG in a quantum dot solar cell. Science *334*, 1530–1533.

43. Hyeon-Deuk, K., and Prezhdo, O. V. (2012). Multiple exciton generation and recombination dynamics in small Si and CdSe quantum dots: An ab initio time-domain study. ACS Nano *6*, 1239–1250.

44. de Weerd, C., Gomez, L., Capretti, A., Lebrun, D.M., Matsubara, E., Lin, J., Ashida, M., Spoor, F.C.M., Siebbeles, L.D.A., Houtepen, A.J., *et al.* (2018). Efficient carrier multiplication in $CsPbI_3$ perovskite nanocrystals. Nat. Commun. *9*, 1–9.

45. Beard, M.C., Midgett, A.G., Hanna, M.C., Luther, J.M., Hughes, B.K., and Nozik, A.J. (2010). Comparing multiple exciton generation in quantum dots to impact ionization in bulk semiconductors: Implications for enhancement of solar energy conversion. Nano Lett. *10*, 3019–3027.

46. Hu, L., Zhao, Q., Huang, S., Zheng, J., Guan, X., Patterson, R., Kim, J., Shi, L., Lin, C.H., Lei, Q., *et al.* (2021). Flexible and efficient perovskite quantum dot solar cells via hybrid interfacial architecture. Nat. Commun. *12*, 1–9.

47. Luo, T., Zhang, Y., Xu, Z., Niu, T., Wen, J., Lu, J., Jin, S., Liu, S., and Zhao, K. (2019). Compositional Control in 2D Perovskites with Alternating Cations in the Interlayer Space for Photovoltaics with Efficiency over 18%. Adv. Mater. *31*, 1903848.

48. Yin, J., Maity, P., Naphade, R., Cheng, B., He, J.H., Bakr, O.M., Brédas, J.L., and Mohammed, O.F. (2019). Tuning Hot Carrier Cooling Dynamics by Dielectric Confinement in Two-Dimensional Hybrid Perovskite Crystals. ACS Nano *13*, 12621–12629.

49. Einzinger, M., Wu, T., Kompalla, J.F., Smith, H.L., Perkinson, C.F., Nienhaus, L., Wieghold, S., Congreve, D.N., Kahn, A., Bawendi, M.G., *et al.* (2019). Sensitization of silicon by singlet exciton fission in tetracene. Nature *571*, 90–94.

50. Thompson, N.J., Congreve, D.N., Goldberg, D., Menon, V.M., and Baldo, M.A. (2013). Slow light enhanced singlet exciton fission solar cells with a 126% yield of electrons per photon. Appl. Phys. Lett. *103*, 263302.

51. Yang, L., Tabachnyk, M., Bayliss, S.L., Böhm, M.L., Broch, K., Greenham, N.C., Friend, R.H., and Ehrler, B. (2015). Solution-processable singlet fission photovoltaic devices. Nano Lett. *15*, 354–358.

52. Lu, H., Chen, X., Anthony, J.E., Johnson, J.C., and Beard, M.C. (2019). Sensitizing Singlet Fission with Perovskite Nanocrystals. J. Am. Chem. Soc. *141*, 4919–4927.

53. Wieghold, S., Bieber, A.S., VanOrman, Z.A., Daley, L., Leger, M., Correa-Baena, J.P., and Nienhaus, L. (2019). Triplet Sensitization by Lead Halide Perovskite Thin Films for Efficient Solid-State Photon Upconversion at Subsolar Fluxes. Matter *1*, 705–719.

54. Tabachnyk, M., Ehrler, B., Gélinas, S., Böhm, M.L., Walker, B.J., Musselman, K.P., Greenham, N.C., Friend, R.H., and Rao, A. (2014). Resonant energy transfer of triplet excitons from pentacene to PbSe nanocrystals. Nat. Mater. *13*, 1033–1038.

55. Luque, A., and Martí, A. (1997). Increasing the Efficiency of Ideal Solar Cells by Photon Induced Transitions at Intermediate Levels. Phys. Rev. Lett. *78*, 5014–5017.

56. Ramiro, I., Marti, A., Antolin, E., and Luque, A. (2014). Review of experimental results related to the operation of intermediate band solar cells. IEEE J. Photovoltaics *4*, 736–748.

57. Egger, D.A. (2018). Intermediate Bands in Zero-Dimensional Antimony Halide Perovskites. J. Phys. Chem. Lett. *9*, 4652–4656.

58. Rasukkannu, M., Velauthapillai, D., and Vajeeston, P. (2018). A first-principle study of the electronic, mechanical and optical properties of inorganic perovskite Cs2SnI6 for intermediate-band solar cells. Mater. Lett. *218*, 233–236.

59. An, J., Jiang, H., Tian, Y., Xue, H., and Tang, F. (2019). Manganese doping mechanism in a CsPbI2Br photovoltaic material: A first-principles study. Phys. Chem. Chem. Phys. *21*, 23552–23558.

60. Sampson, M.D., Park, J.S., Schaller, R.D., Chan, M.K.Y., and Martinson, A.B.F. (2017). Transition metal-substituted lead halide perovskite absorbers. J. Mater. Chem. A *5*, 3578–3588.

61. Ma, X., and Li, Z. (2020). Half-filled intermediate bands in doped inorganic perovskites for solar cells. Phys. Chem. Chem. Phys. *22*, 23804–23809.

62. Marti, A., Cuadra, L., and Luque, A. (2000). Quantum dot intermediate band solar cell. In Conference Record of the IEEE Photovoltaic Specialists Conference (Institute of Electrical and Electronics Engineers Inc.), pp. 940–943.

63. Hosokawa, H., Tamaki, R., Sawada, T., Okonogi, A., Sato, H., Ogomi, Y., Hayase, S., Okada, Y., and Yano, T. (2019). Solution-processed intermediate-band solar cells with lead sulfide quantum dots and lead halide perovskites. Nat. Commun. *10*, 1–8.

64. Liu, S., Zheng, F., Koocher, N.Z., Takenaka, H., Wang, F., and Rappe, A.M. (2015). Ferroelectric domain wall induced band gap reduction and charge separation in organometal halide perovskites. J. Phys. Chem. Lett. *6*, 693–699.

65. Stone, G., Puggioni, D., Lei, S., Gu, M., Wang, K., Wang, Y., Ge, J., Lu, X.-Z., Mao, Z., Rondinelli, J.M., *et al.* (2019). Atomic and electronic structure of domains walls in a polar metal. Phys. Rev. B *99*, 014105.

66. Min, H., Lee, D.Y., Kim, J., Kim, G., Lee, K.S., Kim, J., Paik, M.J., Kim, Y.K., Kim, K.S., Kim, M.G., *et al.* (2021). Perovskite solar cells with atomically coherent interlayers on SnO2 electrodes. Nat. 2021 5987881 *598*, 444–450.

67. Dimroth, F., Tibbits, T.N.D., Niemeyer, M., Predan, F., Beutel, P., Karcher, C., Oliva, E., Siefer, G., Lackner, D., Fus-Kailuweit, P., *et al.* (2016). Four-junction wafer-bonded concentrator solar cells. IEEE J. Photovoltaics *6*, 343–349.

68. Würfel, P. (1997). Solar energy conversion with hot electrons from impact ionisation. Sol. Energy Mater. Sol. Cells *46*, 43–52.

69. Green, M.A. THIRD GENERATION PHOTOVOLTAICS: RECENT THEORETICAL

PROGRESS. Available at:
http://citeseerx.ist.psu.edu/viewdoc/download?doi=10.1.1.573.6314&rep=rep1&type=pdf
[Accessed May 10, 2021].

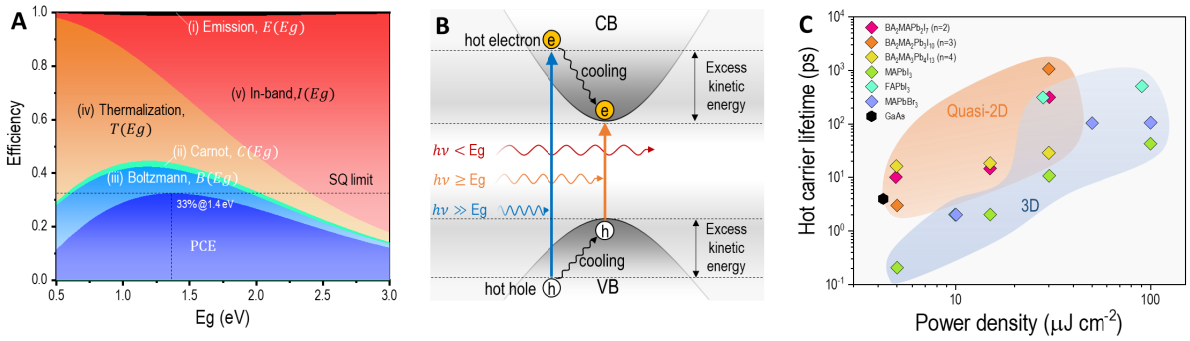

Figure 1 (A) Intrinsic loss mechanisms in an ideal single junction PV cell, with respect to E_g. Five losing pathways include (i) Emission, $E(Eg)$; (ii) Carnot, $C(Eg)$; (iii) Boltzmann, $B(Eg)$; (iv) Thermalization, $T(Eg)$; (v) In-band,$I(Eg)$, with a correlation of $E(Eg) + C(Eg) + B(Eg) + T(Eg) + I(Eg) + PCE(Eg) = 100\%$. **(B)** Band diagram showing the thermalization ($h\nu \gg Eg$, coupled with hot carrier relaxation/cooling dynamics) and in-band ($h\nu < Eg$) losses. **(C)** Hot carrier cooling time for typical semiconductor of GaAs, three-dimensional (3D) perovskites and (quasi) two-dimensional (2D) perovskites. Data points are collected from reference 11, 16, 17.

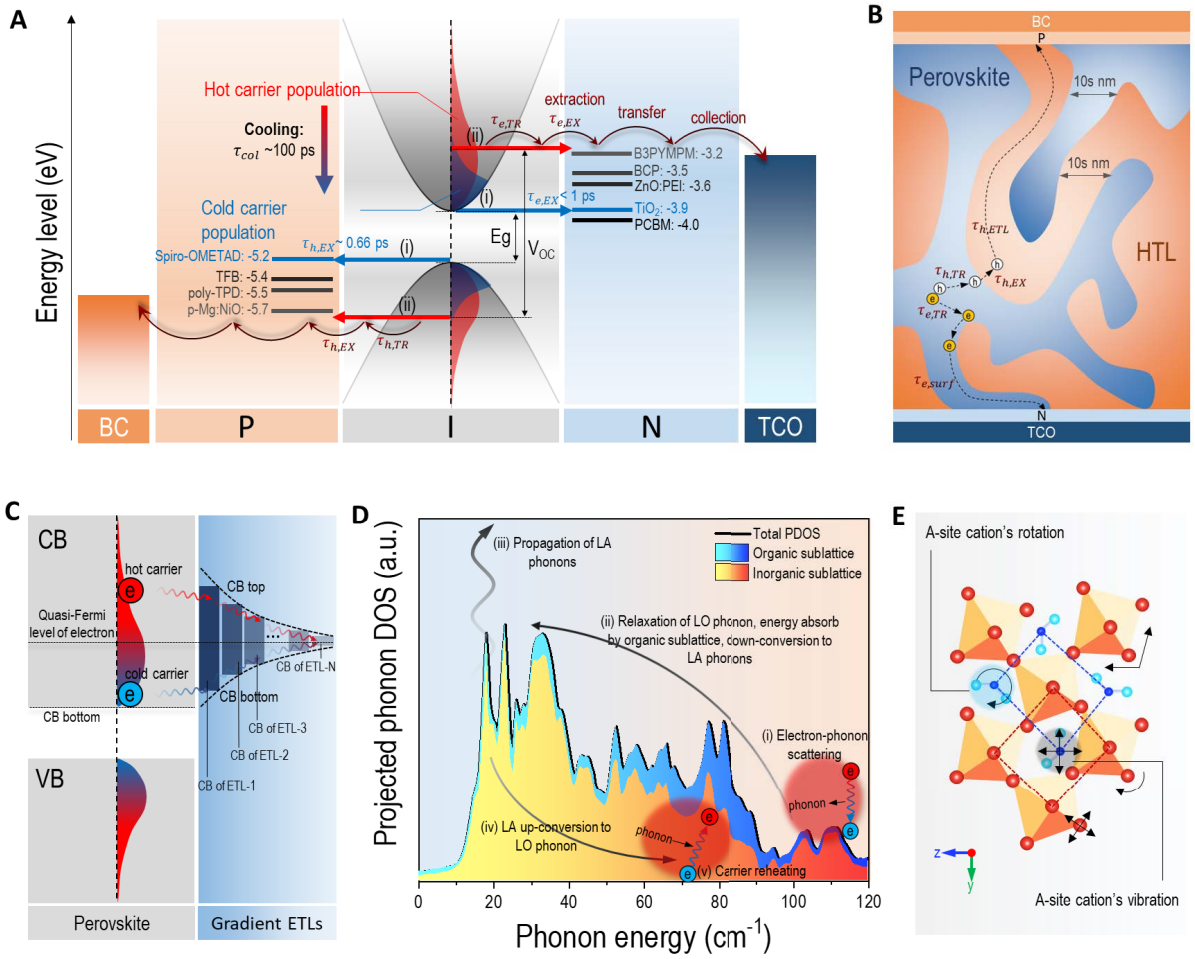

Figure 2 (A) Photophysical process in an n-i-p single junction solar cell, where TCO is transparent conductive oxide, BC is back contact, and multiple n-type and p-type example materials with energy level form -3.2~-4.0 eV and -5.2~-5.7 eV are listed, respectively. For solar cell application, photocarriers need to firstly transport through the perovskite, then be extracted by electron/hole transfer layer, and further transfer to electrodes to be collected. (i) Cold carrier extractions by TiO_2 and Spiro-OMeTAD in regular solar cell; (ii) hot carrier extraction by decent level electron/hole transfer layer. **(B)** Bulkheterojunction design of bi-continuous phase of perovskite and HTL with a phase separation of 10s nm in order to save diffusion distance for hot carriers. Hot holes could be quickly extracted to HTL and transfer within HTL to anode; hot electrons could transfer along the perovskite phase surface to cathode. **(C)** A gradient ETLs design to simultaneously extract both the cold and hot carriers to ETLs so that a resultant quasi-Fermi level of electrons could be higher than the CBM of perovskite. **(D)** Proposed phonon dynamics in a $FAPbI_3$ perovskite, adapted with permission from Jianfeng Yang *et al* (ref. 27), copyright Springer Nature © 2017. The total phonon DOS is contributed by both inorganic and organic sub-lattices. **(E)** Dynamics of inorganic and organic sub-lattices.

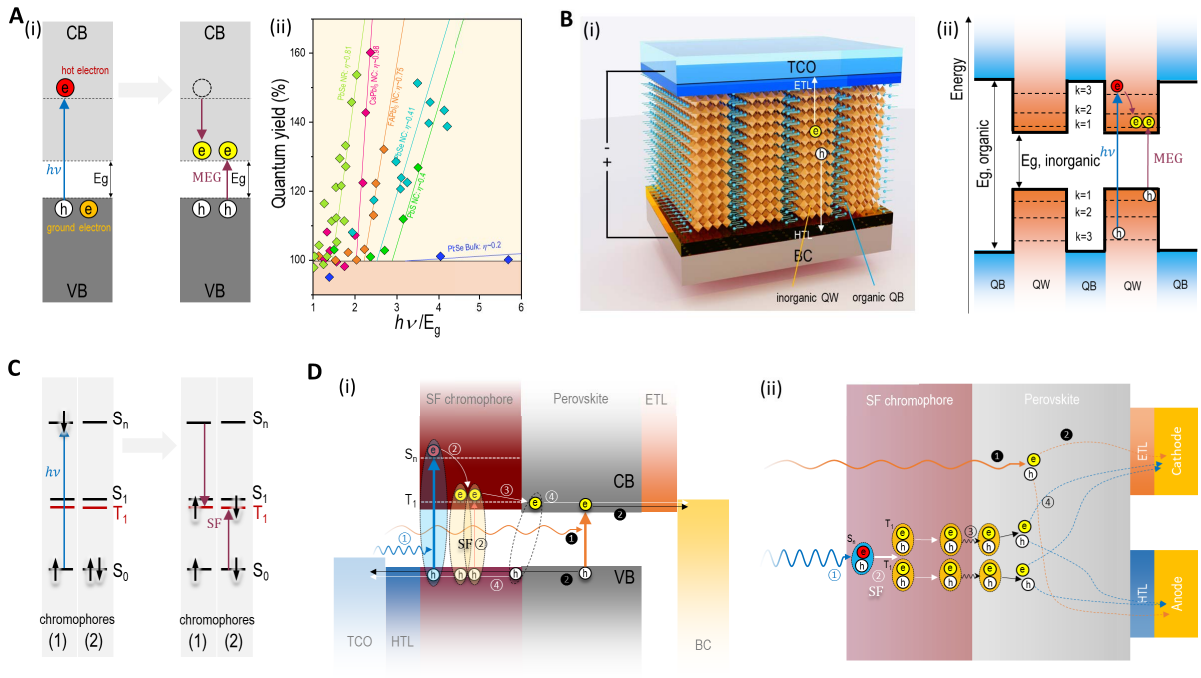

Figure 3 (A) (i) Typical MEG process: higher energy photon excites a VB electron to high energy level in CB with excess of kinetic energy, which is used for another VB electron's excitation to CB. **(ii)** Plot of quantum yield (number ratio of electron–hole pairs over absorbed photons) vs. photon energy, for perovskite and typical MEG QD materials. **(B)** Utilization of MQW quasi-2D perovskite for MEG solar cell. **(i)** An exemplified device structure of transparent conductive oxide (TCO)/electron transfer layer (ETL)/vertically aligned quasi-2D perovskite/hole transfer layer (HTL)/back contact (BC). The electron and hole could vertically transfer within the inorganic QW (quantum well) plane. **(ii)** Energy band diagram of quasi-2D perovskite. Quantum confinement is listed here to show quantized energy level in the QW region, where the MEG could occur. **(C)** Typical SF process: spin-allowed conversion of one singlet exciton to two triplet excitons. **(D)** Utilization SF chromophore for SF perovskite solar cell *via* **(i)** 'charge transfer' and **(ii)** 'energy transfer' mechanisms across the SF chromophore/perovskite interface. **(i)** Energy diagram showing a 'charge transfer' working principle: SF chromophore absorbs short-wavelength light that ① excites electron to S_n to form one singlet exciton, followed by ② SF-induced formation of two triplet excitons, which ③ diffuse to the chromophore/perovskite interface, ④ dissociate into free carriers at the interface and transport all the way to corresponding electrodes *via* pathways of perovskite/ETL/BC for electrons and chromophore/HTL/TCO for holes, respectively. Meanwhile, perovskite absorbs long-wavelength light that ❶ excites VB electrons to CB of perovskite, followed by ❷ transport to corresponding electrodes. **(ii)** Illustration of an 'energy transfer' working principle in a lateral device: SF chromophore absorbs short-wavelength light that ① excites electron to S_n to form one singlet exciton, followed by ② SF-induced formation of two triplet excitons, which induce the formation of excitons in perovskite *via* ③ energy transfer process. Due to the small exciton binding energy in perovskite, room temperature thermal energy could separate the excitons into free carriers, followed by ④ transfering towards corresponding electrodes. Meanwhile, perovskite ❶ absorbs long-wavelength light where photocarriers ❷ transport to corresponding electrodes.

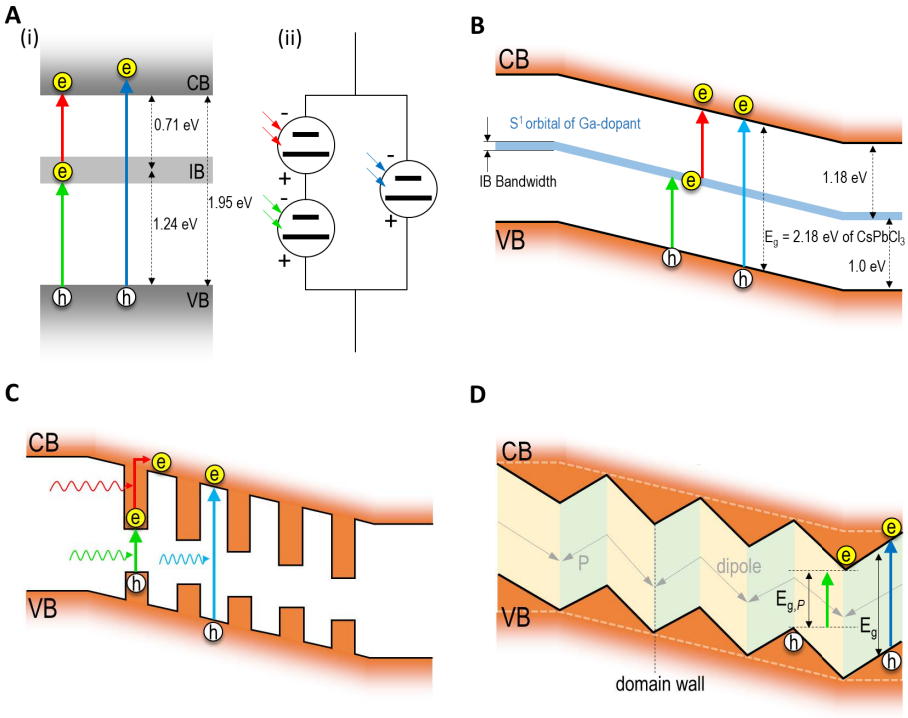

Figure 4 Sub-bandgap photophysical process. (A) (i) An ideal band diagram of a semiconductor with intermediate band (IB), with VB-IB sub gap of 1.24 eV and IB-CB of 0.71 eV, respectively. **(ii)** Equivalent electrical circuit of an IB solar cell to illustrate the transitions. Proposed IB solar cells based on **(B)** extrinsically doped $CsPbCl_3$ with IB formed by S^1 orbital of Ga-dopant, and **(C)** a MQW quasi-2D perovskite or composite consisting of QD being embedded in a wide E_g perovskite matrix. **Photoferroic solar cell. (D)** Polarization induced ferroelectric domain in a perovskite, leading to localized energy level change, which could offer lower $E_{g,P}$ across the domain wall.